Exploring Laminar Iron-Flame Propagation Limits in Long, Narrow Channels

Swagnik Guhathakurta[a], Daniel Mira[b], Jeroen van Oijen[a]
[a]Eindhoven University of Technology, Eindhoven, Netherlands
[b]Barcelona Supercomputing Center, Barcelona, Spain

1 Introduction

As the demand for energy keeps rising worldwide, so does the push toward renewable and clean energy sources. The problem with most renewable energy sources, such as solar and wind, is that they are location and time-dependent. Thus the storage and safe transportation of energy are key. In 2018, Bergthorson [1] proposed that metal fuels can be a promising carbon-free energy carrier. He also identified that the physical properties of iron particles make it one of the best metals suitable for this application - during the combustion of iron, the particle never exceeds the boiling point. Therefore the entire reaction process occurs in the heterogeneous phase and at the surface of the particles. The combustion results in micron-sized particles of iron oxide that can be easily captured and reduced back to iron particles using renewable energy. Another benefit to using iron particles is that the storage and transportation of these particles are relatively easy and safe.

Many researchers around the globe have been interested in metal particle combustion for quite some time. However, the combustion of iron particles is a relatively new research topic. In order to optimize and design practical combustors that use iron powders, a basic understanding of the nature of combustion is essential. Some of the recent studies on iron particle burning reveal the mysteries of this unique nature of combustion [2–7]. Currently, iron particle combustion research can be divided into two broad categories - research on single particle combustion behavior, and the nature of flame propagation in iron clouds suspended in a gas. Most of the research in the second category right now is experimental work, though there has been a push toward numerical simulations in recent times. In the research work presented here, quasi-one-dimensional simulations of iron flame propagation were carried out using an Eulerian-Lagrangian framework in Alya to explore the lean and rich flame propagation limits in a long and narrow channel.

2 Problem Description and Numerical Models

Figure 1 shows the numerical setup that is used in this study. The computational domain is a 5 cm long channel with a height and width of 2 mm. The left end is open while the right end is closed. The walls of the channel have a slip-wall boundary condition. Starting at the left boundary, the first 1 cm of the channel is initialized with hot air and pre-suspended particles at 850 K. The rest of the channel has cold

Correspondence to: s.g.guhathakurta@tue.nl

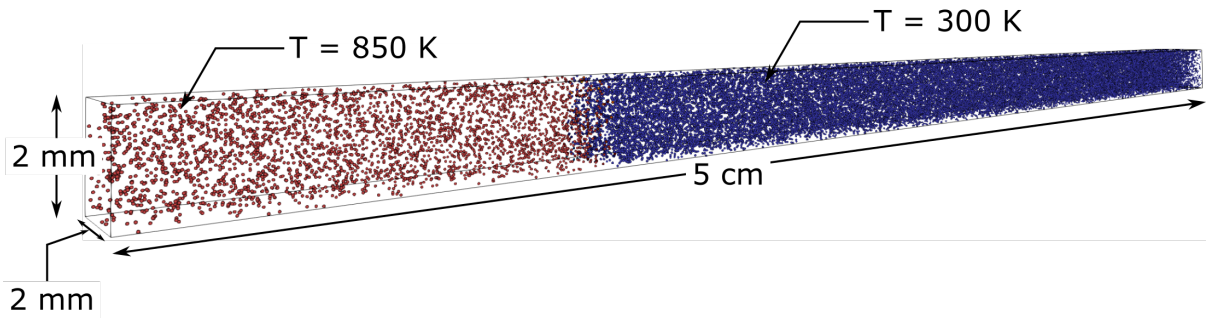

Figure 1: Initial conditions of the numerical setup.

air and particles at 300 K. The number of particles in the channel is calculated from the equivalence ratios and the air density. Due to the higher temperature and thus lower air density, the number of particles in the hot region is lower than in the cold region. Initially, all particles are unreacted - pure iron. The iron particles are assumed to be spherical and monodisperse with $10\,\mu\mathrm{m}$ diameter, have a constant specific heat capacity of 677 J/kg.K, and an unburnt material density, ρ_u, of 7874 kg/m^3 for pure iron. After combustion, the particles are assumed to convert to wustite (FeO), with a burnt material density, ρ_b of 5745 kg/m^3.

2.1 Particle model

The particle and reaction models used in this study are similar to the work by Hazenberg & van Oijen [2]. Since the flame temperature of iron in air (∼2200 K) is less than the boiling point of iron (∼3100 K) and its oxide (∼3400 K), the reaction is assumed to occur only in the heterogeneous mode. The position x_p and velocity u_p of each of the particle is tracked in time using a Lagrangian formulation,

$$\frac{dx_\mathrm{p}}{dt} = u_\mathrm{p}, \frac{du_\mathrm{p}}{dt} = \frac{3}{4}\frac{C_D\rho}{d_\mathrm{p}\rho_\mathrm{p}}|u-u_\mathrm{p}|(u-u_\mathrm{p}). \tag{1}$$

Neglecting gravity, the drag forces are computed using,

$$\frac{du_\mathrm{p}}{dt} = \frac{1}{\tau_\mathrm{p}}(u-u_\mathrm{p}), \tag{2}$$

where τ_p is the relaxation time which indicates how fast the particle velocity adjusts to the gas velocity. Combining Eqs. (1) and (2), we get

$$\tau_\mathrm{p} = \frac{4}{3}\frac{\rho_\mathrm{p} d_\mathrm{p}}{\rho C_d}\frac{1}{|u-u_\mathrm{p}|}. \tag{3}$$

The Schiller & Naumann [8] drag coefficient C_d and the Reynolds number Re are given as

$$C_d = \frac{24}{Re}(1+0.15Re^{0.687}), \quad Re = \frac{\rho|u-u_\mathrm{p}|d_\mathrm{p}}{\mu}, \tag{4}$$

where d_p is the particle diameter, ρ is the gas density and μ is the gas dynamic viscosity. Particle properties are denoted by subscript p, whereas gas properties have no subscript unless otherwise noted.

Single-step heterogeneous surface chemistry was assumed for the chemical reactions,

$$2\,\mathrm{Fe} + \mathrm{O_2} \longrightarrow 2\,\mathrm{FeO}$$

The reaction rate of this surface reaction is modeled by an Arrhenius type equation,

$$k_r = k_0 \exp\left(\frac{-E_a}{R_u T_\mathrm{p}}\right), \tag{5}$$

where k_r is the surface reaction rate, k_0 is the pre-exponential factor, E_a is the activation energy, R_u is the universal gas constant, and T_p is the particle temperature, which is assumed to be uniform over the entire particle. Due to the heterogeneous nature of the reaction, the oxygen from the surrounding gas has to diffuse to the particle surface. Depending on the conditions, the reaction rate can be limited either by surface kinetics or external diffusion of oxygen. The mass consumption rate ω of oxygen is a combination of diffusion-limited and kinetic-limited regimes. The rate at which the mass of the particle m_p and the unreacted iron mass $m_\mathrm{p,Fe}$ change with time are given by

$$\frac{dm_\mathrm{p}}{dt} = \omega \cdot \pi d_\mathrm{p}^2, \quad \frac{dm_\mathrm{p,Fe}}{dt} = -\frac{1}{s}\frac{dm_\mathrm{p}}{dt}, \tag{6}$$

where s is the mass-based stoichiometric ratio. The rate of change of particle enthalpy H_p due to convective heat transfer and the reaction with oxygen can be written as

$$\frac{dH_\mathrm{p}}{dt} = k_\mathrm{c} A_\mathrm{p}(T_\mathrm{p} - T) + \frac{dm_\mathrm{p}}{dt} h_{\mathrm{O}_2}, \tag{7}$$

where k_c is the convective heat transfer coefficient, T is the surrounding gas temperature, T_p is the particle temperature, h_{O_2} is the enthalpy of oxygen. k_c is given by

$$k_\mathrm{c} = Nu\, \lambda_\mathrm{f}/d_\mathrm{p}, \tag{8}$$

where λ_f is the thermal conductivity in the film layer and Nu is the Nusselt number which is assumed to be constant ($Nu = 2$). Various simulation parameters used in this work are given in Table 1.

Table 1: Parameters of the iron-particle model.

Parameter	Value	Units	Description
s	0.28	-	Mass-based stoichiometric ratio
ρ_u	7 874	kg/m^3	Iron density
ρ_b	5 745	kg/m^3	FeO density
C_p	677	J/(kg K)	Specific thermal capacity of Fe and FeO
Δh_c	2.906×10^6	J/kg	Specific energy release
k_∞	75.0×10^5	m/s	Pre-exponential factor
E_a/R_u	14.4×10^3	K	Activation temperature

2.2 Gas model

For the gas-phase modeling, the Navier-Stokes equations with a low-Mach number approximation are solved in Alya [9] for the continuity, momentum, energy, and species mass conservation. The details of these equations are given in Both et al. [10], with a slight modification that no Large Eddy Simulation (LES) filters are being used in this work since the cases are all laminar. The results presented in this paper use constant gas-phase transport properties (conductivity, viscosity, and diffusion coefficients) that are evaluated at a temperature of $T_g = 300\,\mathrm{K}$, although the final paper will report the results using realistic, temperature-dependent fluid properties.

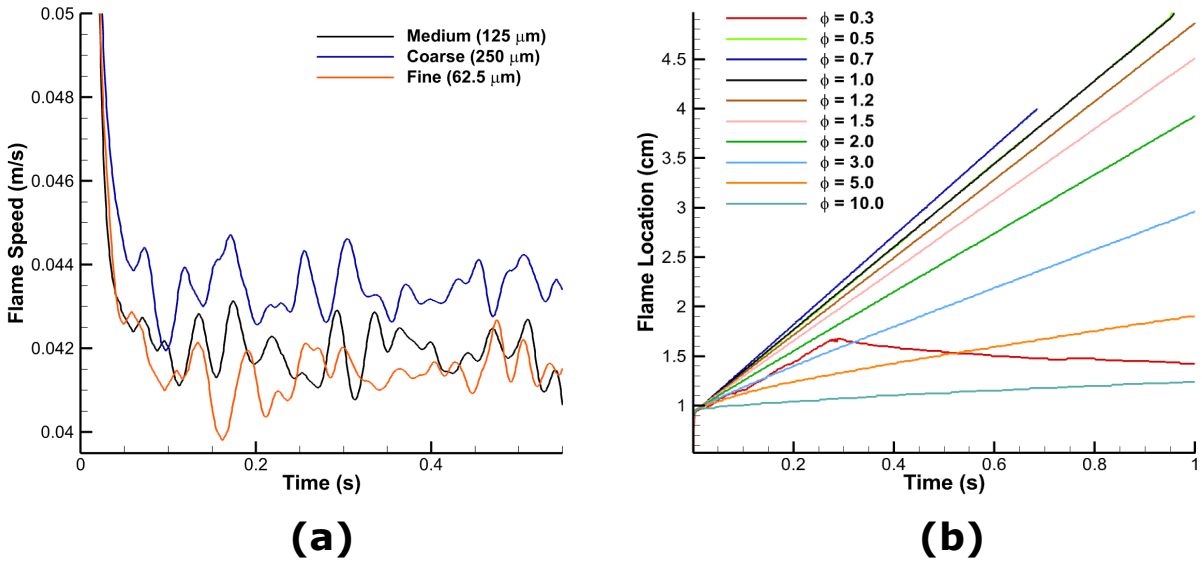

Figure 2: (a) Flame speeds for three different grid spacings of $125\,\mu\mathrm{m}$ (medium), $62.5\,\mu\mathrm{m}$ (fine), and $250\,\mu\mathrm{m}$ (coarse); (b) flame location vs. time for the entire range of equivalence ratios

3 Results and Discussion

Initial verification of the particle model in Alya was performed using a single-particle, one-way coupled iron particle combustion, where we assume that the gas phase is not affected by the particle phase. For validation, the laminar flame propagation speeds from Alya were compared to Chem1D [11], ensuring that the models are exactly the same. We also performed grid convergence tests to make sure that the results are grid-independent. Figure 2 (a) shows the flame speeds for three different grid spacings of $125\,\mu\mathrm{m}$ (medium), $62.5\,\mu\mathrm{m}$ (fine), and $250\,\mu\mathrm{m}$ (coarse). The flame speeds for the medium and fine are quite similar, whereas, with the coarse grid, the speeds are slightly higher. Thus, the medium grid size was chosen for all the simulations presented here. Note that these simulations were performed using only one cell per direction in the y- and z-directions (transverse to the flame propagation direction). This is required because Lagrangian particles can only be used in 3-D simulations in Alya. Thus, having only one cell in the transverse directions enables us to run the quasi-1-D simulations. Alya is a Finite Element code, and therefore, there are still very minor variations in the transverse directions because the values are stored at the nodes and not cell centers like in Finite Volume codes.

Next, we performed several simulations with various equivalence ratios (denoted by ϕ) in the range of 0.3 to 10 to find the flame propagation limits in lean and rich conditions. Figure 2 (b) shows the flame locations for equivalence ratios of 0.3, 0.5, 0.7, 1.0, 1.2, 1.5, 2.0, 3.0, 5.0, and 10.0. The flame fronts are tracked by finding the location where the gradient of the oxygen mass fraction is maximum. The flame propagation is stable for all the cases except for $\phi = 0.3$. At $\phi = 0.3$, the propagation is highly erratic and stops after ~ 0.3 seconds. Thus, we could not calculate the flame speed or adiabatic flame temperatures for this case. The flame temperature just before the flame propagation fails for this case is ~ 1000 K, which is still higher than the particle ignition temperature. However, the time the particles take to ignite is longer than in other cases. By the time the particles ignite, they have already moved quite far from the unburnt particles and thus are not able to conduct the heat effectively to the cold particles. When the flame propagation stops, the particles are only able to reach a temperature of about 800 K, which is not enough to ignite the particles.

Figure 3 (a) shows the time-evolution of the laminar flame speeds for all values of ϕ, except for 0.3,

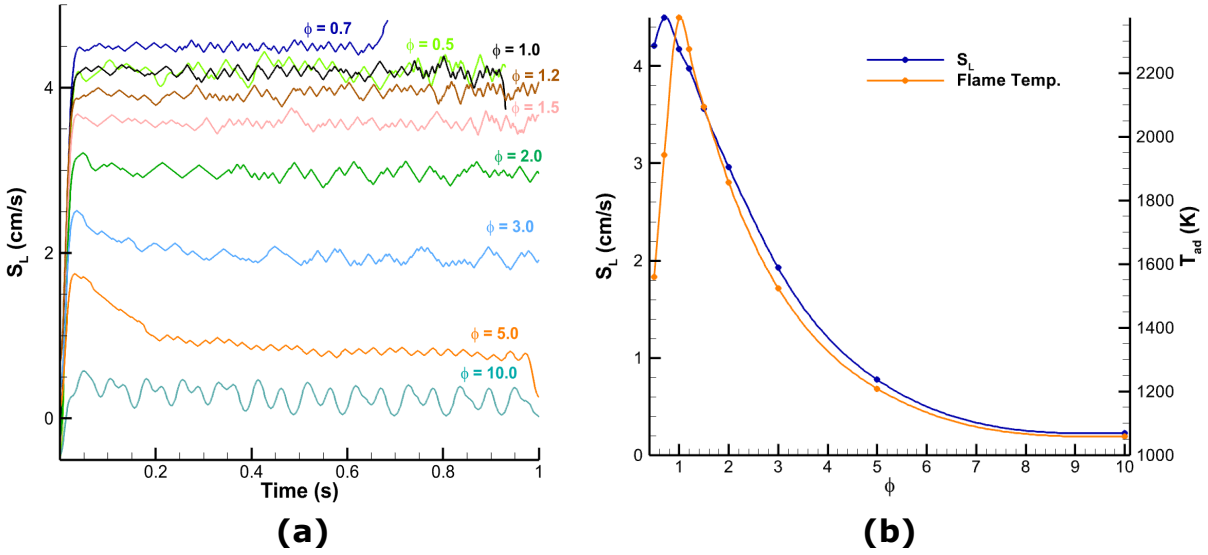

Figure 3: (a) Laminar flame speeds vs. time for the entire range of equivalence ratios ϕ, (b) mean laminar flame speeds and adiabatic flame temperatures vs. equivalence ratio ϕ.

and Figure 3 (b) shows the mean flame speeds and adiabatic flame temperatures. Note that the adiabatic flame temperatures reported here for ϕ = 5 and 10 were the values at the end of the simulation ($\sim$ 1 second) because the flame temperatures for these cases keep reducing with time. The overall trends for the flame speeds and the flame temperatures agree well with the previous work from Hazenberg & van Oijen [2]. The maximum flame speed of 4.49 cm/s was observed at $\phi = 0.7$, and the maximum adiabatic flame temperature of 2374 K was at ϕ = 1. However, the flame speeds shown here are lower than those in Hazenberg & van Oijen, primarily due to the fact that we use constant fluid properties that are evaluated at 300 K. We are currently repeating these simulations using realistic temperature-dependent fluid properties, which will be included in the final paper.

We were not able to directly determine the flammability limit for rich conditions due to the computational cost. When $\phi = 5$, the number of particles is more than 200,000 particles, each of which is tracked individually. Reducing the width and depth of the channel would allow us to go to a higher equivalence ratio while maintaining the same number of particles, and this is part of our ongoing work. For ϕ = 5 and 10, we already observe that the flame speeds are very low, indicating that the rich limit is close to ϕ = 10. The flames still propagate because they are adiabatic and the flame temperatures are higher than the ignition temperature. Note that at these higher values of ϕ, the medium can be considered to be optically thick. In these cases, radiation may have an impact on flame propagation. However, we neglect radiation heat transfer in these simulations.

4 Conclusions

Numerical simulations of quasi-one-dimensional flame propagation were performed for pre-suspended iron particles in air. We looked at a wide range of equivalence ratios (0.3 to 10) to determine the lean and rich limits for flame propagation. From the results, we observe that the flame gets quenched for an equivalence ratio of 0.3. However, in the rich case, we were not able to directly determine the limit due to computational costs associated with tracking a massive number of particles individually. The overall trends of flame temperature and flame speeds versus equivalence ratio matched well with previous work from Hazenberg & van Oijen [2], but the actual values are different due to the constant

gas phase properties that are used in this model. Determining more realistic values using temperature-dependent fluid properties is part of our ongoing work. Future work will also include investigating the flammability limit under rich conditions using equivalence ratios higher than 10 and using smaller steps in the equivalence ratio range to improve the accuracy of the prediction.

5 Acknowledgements

This work was supported by the European Union Center of Excellence in Combustion (CoEC) project. The authors acknowledge the Eindhoven University of Technology supercomputing resources that were used for this research and the Barcelona Supercomputing Center for providing access to their code Alya.

References

[1] Bergthorson, J. M. (2018). Recyclable metal fuels for clean and compact zero-carbon power. Progress in Energy and Combustion Science, 68, 169-196.

[2] Hazenberg, T., & van Oijen, J. A. (2021). Structures and burning velocities of flames in iron aerosols. Proceedings of the Combustion Institute, 38(3), 4383-4390.

[3] Tang, F. D., Goroshin, S., & Higgins, A. J. (2011). Modes of particle combustion in iron dust flames. Proceedings of the Combustion Institute, 33(2), 1975-1982.

[4] Thijs, L. C., van Gool, C. E. A. G., Ramaekers, W. J. S., van Oijen, J. A., & de Goey, L. P. H. (2022). Resolved simulations of single iron particle combustion and the release of nano-particles. Proceedings of the Combustion Institute.

[5] Ning, D., Shoshin, Y., van Oijen, J. A., Finotello, G., & De Goey, L. P. H. (2021). Burn time and combustion regime of laser-ignited single iron particle. Combustion and Flame, 230, 111424.

[6] Li, S., Huang, J., Weng, W., Qian, Y., Lu, X., Aldén, M., & Li, Z. (2022). Ignition and combustion behavior of single micron-sized iron particle in hot gas flow. Combustion and Flame, 241, 112099.

[7] McRae, M., Julien, P., Salvo, S., Goroshin, S., Frost, D. L., & Bergthorson, J. M. (2019). Stabilized, flat iron flames on a hot counterflow burner. Proceedings of the Combustion Institute, 37(3), 3185-3191.

[8] Schiller, L. (1933). Über die grundlegenden Berechnungen bei der Schwerkraftaufbereitung. Z. Vereines Deutscher Inge., 77, 318-321.

[9] Vázquez, M., Houzeaux, G., Koric, S., Artigues, A., Aguado-Sierra, J., Arís, R., ... & Valero, M. (2016). Alya: Multiphysics engineering simulation toward exascale. Journal of computational science, 14, 15-27.

[10] Both, A., Mira Martínez, D., & Lehmkuhl Barba, O. (2022). Assessment of tabulated chemistry models for the les of a model aero-engine combustor. In Proceedings of Global Power and Propulsion Society, GPPS Chania22, 18th-20th September, 2022. Global Power and Propulsion Society (GPPS).

[11] Somers, L. M. T. (1994). The simulation of flat flames with detailed and reduced chemical models, Doctoral dissertation, Eindhoven University of Technology.